Journal of Cluster Science
https://doi.org/10.1007/s10876-019-01507-w

ORIGINAL PAPER

A Systematic Study of Cu Nanospheres Embedded in Non-ionic Surfactant-Based Vesicle: Photocatalytic Efficiency and In Vivo Imaging Study

Hojjat Samareh Fekri[1] · Mehdi Ranjbar[2] · Abbas Pardakhty[2]

Received: 26 November 2018

Abstract
In this study, for the first time nanoparticles were synthesized and encapsulated in non-ionic surfactant-based vesicle (biology and chemistry). The non-ionic surfactant-based vesicle is formed mostly by non-ionic surfactant and cholesterol incorporation as an excipient by green capping agent. We researched a novel processing route for produce Cu nanospheres encapsulated in a non-ionic surfactant-based vesicle by glucose as a green capping reductant with microwave assisted reverse micelle method. The effect of glucose concentration and microwave power on the morphology, particle size, distribution and in vitro photoluminescence spectroscopy experiments of nanoparticles entrapped in the non-ionic surfactant-based vesicles were investigated. The synthesis parameters in this study were designed by Taguchi technique and various factors such as glucose concentration, temperature, microwave power and interaction between these factors were studied. The metal nanostructure with photocatalytic activity act as an emerging, non-invasive therapeutic strategy that involves photosensitizer drugs and external light for the treatment of cancer. The products were characterized by XRD, SEM, TEM, DLS, TGA and UV–Vis. The current study points out a successful example of using Cu nanospheres embedded in non-ionic surfactant-based vesicle as a new and novel nanomedicine material for in vivo imaging and the photocatalytic efficiency of methylene blue.

✉ Mehdi Ranjbar
Mehdi.Ranjbar@Kmu.ac.ir

[1] Student Research Committee, Kerman University of Medical Sciences, Kerman, Iran

[2] Pharmaceutics Research Center, Institute of Neuropharmacology, Kerman University of Medical Sciences, P.O. Box 76175-493, Kerman 76169-11319, Iran

Published online: 14 February 2019

Graphical Abstract

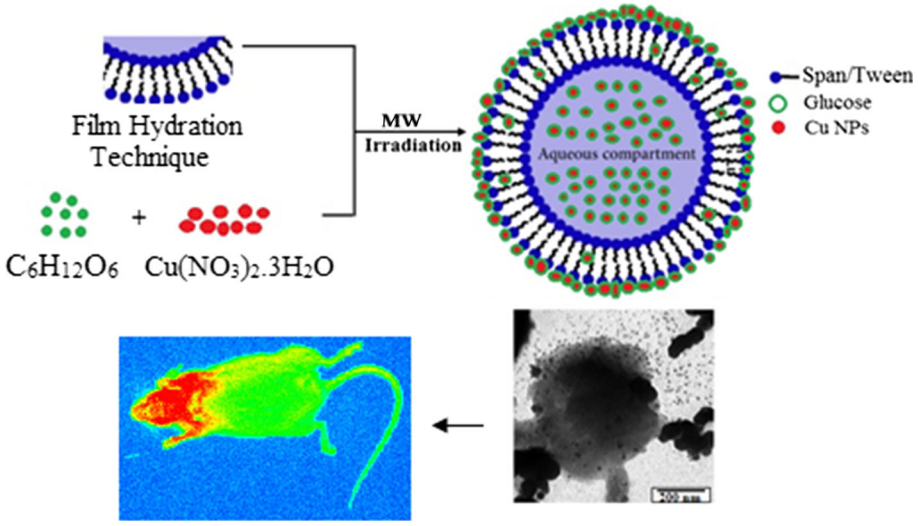

Keywords Cu nanospheres · Encapsulation · In vivo imaging · Reverse micelle

Introduction

Recently nanoparticles and niosomes delivery system have been proposed as colloidal drug carriers [1–3]. There is a growing need to develop reactions for materials synthesis that do not use detrimental, toxic chemicals. Green/biological NPs have been extensively used in biomedical applications [4–6]. Nanoparticles (NP) are a type of colloidal drug delivery system comprising particles with a size range from 10 to 1000 nm in diameter. In recent years, much attention has been paid to the provision of nanoparticles as carriers for drug delivery. Nanoparticle carriers, by changing the pharmacokinetic properties of the drug [7], improve the function of the drug and reduce its side effects [8]. Metal nanoparticles as super photocatalysts are suitable for in vivo multicolor fluorescence imaging as a novel structures to co-deliver therapeutic agents with photo thermal agents, will have an enormous potential for future diagnosis and therapy [9]. Metallic nanoparticles such as Au, Ag, Pt, and Pd have been widely used in many biomedical applications, separation [10, 11], diagnostics [12] and pharmaceuticals sciences [13, 14]. There are many approaches for synthesis metal nanoparticles for use in medicine and pharmacy, microwave-assisted synthesis [15], hydrothermal [16], solvent-free synthesis [17], citrate precursor method [18], sol–gel methods with several organic precursors [19], green synthesis methodology creates many chemical and physical advantages such as environment friendly, cost effective and easily scaled up for large scale syntheses of nanoparticles, also to do the reactions, there is no need to use high temperature, pressure, energy and toxic chemicals [20–22]. Quantum dots and nanoparticles with high optical properties have unique potential for applications in biological sciences and observation intracellular events in different concentration such as 5% w/w, 10% w/w, 15% w/w the results showed the [23, 24]. The variation in the wavelengths of nanocrystals can be utilized in these structures at the same time, several indicators are present in the living cell components and see the processes inside the cells, the results showed that with change pH to 8 the size of the nanoparticles became homogeneous [25]. In this study we used glucose as capping agent and reductant for reducing Cu(II) to Cu(0) in reactions, noisome structures were prepared by the lipid film hydration technique [26, 27], then Cu nanoparticles were encapsulated in niosomes with microwave assisted reverse micelle method and used for in vivo imaging study. The final products were characterized by XRD, SEM, TEM, TGA and UV–Vis analysis. In this work, for preparation of non-ionic surfactant-based vesicle span/tween 40, 60 and 80 were as surfactant and cholesterol as the lipid phase that non-ionic surfactant-based vesicles have been used for encapsulation Cu nanoparticles. The size of optimized nanostructures in the presence of glucose was about 130- 150 nm. Finally, the efficiency of Cu nanospheres encapsulation in niosomes was investigated to study the optical properties for in vivo imaging effects. The main goal of this project is to achieve targeted nanowires with high-efficiency photocatalytic activity imaging-low-cost treatment and low cost. The optical property of nanostructures as a photocatalyst for the decolorization of methylene blue and also in vivo imaging of

the niosomes containing Cu nanoparticles was measured by UV–Vis spectroscopy and the band gap value was calculated.

Experimental

Chemicals and Equipment

More materials used in this study such as NaOH, $C_6H_{12}O_6$ (Glucose) and Copper(II) nitrate were used as received, without further purification. The nonionic surfactants used as vesicle forming materials were sorbitan monopalmitate (Span 40), sorbitan monostearate (Span 60), sorbitan oleate (Span 80), polyoxyethylene sorbitan monopalmitate (Tween 40), polyoxyethylene sorbitan monostearate (Tween 60), polysorbate 80 (Tween 80) and cholesterol, which were purchased from Fluka (Switzerland). Several analyzes were used to identify the products, such as TGA and DSC were turned from room temperature to 800 °C with a heating rate of 10 °C/min under an argon atmosphere using SCINCO thermal gravimeter S-100 (Seoul, Korea) and Netzsch QMS403C (Selb, Germany). X-ray diffraction (XRD) patterns were recorded by a Philips-X'PertPro, X-ray diffractometer using Ni-filtered Cu Kα radiation at scan range of $10 < 2\ h < 80$, SEM images and DLS diagrams were obtained on LEO-1455VP equipped with an energy dispersive X-ray spectroscopy in Razi Metallurgical Research Center (RMRC). TEM images were obtained on a Philips EM_208S transmission electron microscope with an accelerating voltage of 100 kV. In vivo imaging obtained with in vivo imaging system F Pro model Kodak manufacturing company in USA.

Preparation of Non-ionic Surfactant-Based Vesicle Structures

In a typical approach, niosomes are being prepared by the lipid film hydration technique [28]. For this purpose, the mixtures of a non-ionic surfactant (Span, Tween-40, 60, 80) and cholesterol, with different percentage ratio were dissolved in 10 ml of distilled water in a round bottomed flask. The solvent was evaporated to dryness in a rotary evaporator under reduced pressure at room temperature. During drying, the flask was rotated at 100 rpm speed until a smooth dry lipid film layer was obtained. It was kept 48 h in a vacuum desiccator. The film contains non-ionic surfactant-based vesicle was hydrated using double distilled water. The combination of the prepared vesicles is shown in Table 1.

Preparation of Cu Nanospheres Embedded in Non-ionic Surfactant-Based Vesicle

Copper nanospheres were synthesized by reduction of copper(II) nitrate with glucose as green capping reductant, in a typical and new method 50 mg of $Cu(NO_3)_2$ solved in 10 ml ethylene glycol, then 5 mL of $C_6H_{12}O_6$ (Glucose) at different concentrations inclusive 0.5 mg, 1 mg, and 1.5 mg were subsequently added to the solution under vigorous stirring at 50 °C temperature for 120 min. In the next step, the above solution was added to the made non-ionic surfactant-based vesicle as in situ under reflux system at 50 °C for 180 min. A clear milky suspension was loaded into a microwave Teflon container, and the reactions were performed in a microwave system under various irradiation and time conditions. After microwave irradiation the system was allowed to cool to room temperature naturally then final products were characterized and photoluminescence properties studied (Scheme 1).

Table 1 Summery of conditions for the combination of the prepared niosomes

Formulation	Glucose Con	MW (W)	Cholestrol%	Tween 40%	Span 40%	Span 60%	Tween 60%	Span 80%	Tween 80%
$C_{50}S40_{25}T40_{25}$	0.5	180	50	25	25				
$C_{40}S40_{30}T40_{30}$	1	600	40	30	30				
$C_{30}S40_{35}T40_{35}$	1.5	900	30	35	35				
$C_{50}S60_{25}T60_{25}$	0.5	180	50			25	25		
$C_{40}S60_{30}T60_{30}$	1	600	40			30	30		
$C_{30}S60_{35}T60_{35}$	1.5	900	30			35	35		
$C_{50}S80_{25}T80_{25}$	0.5	180	50					25	25
$C_{40}S80_{30}T80_{30}$	1	600	40					30	30
$C_{30}S80_{35}T80_{35}$	1.5	900	30					35	35

Scheme 1 Summary of experimental route for the synthesis of Cu nanospheres embedded in niosomes

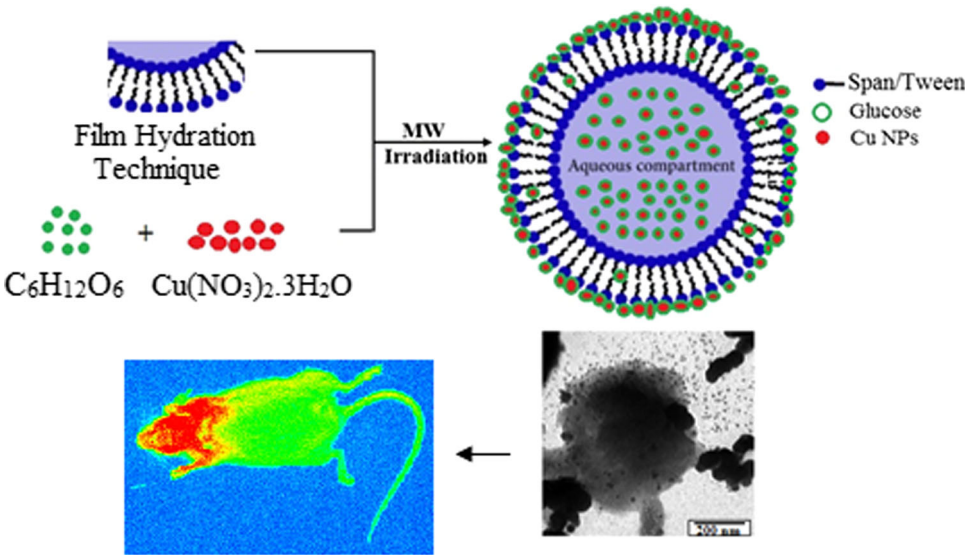

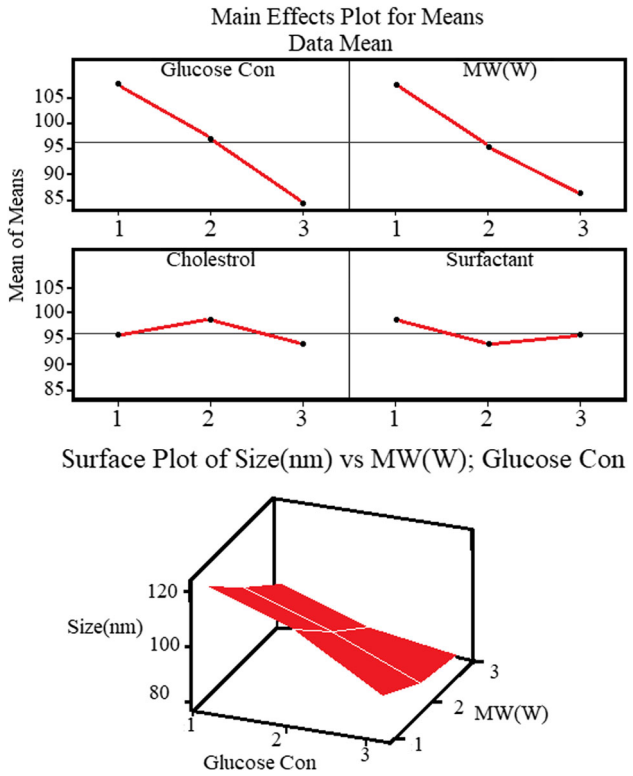

Fig. 1 The statistical diagrams of microwave power, glucose concentration, the percentage of cholesterol and surfactant on particles size parameter with Taguchi technique

Taguchi Technique

To optimize the experiments and factors we employed Taguchi technique, In statistics, a full factorial experiment is an experiment whose design consists of two or more factors, and whose experimental units take on all possible combinations of these levels across all such factors [29]. An experimental design can or randomized clinical trial requires careful consideration of several factors before actually doing the experiment, such an experiment allows the investigator to study the effect of each factor on the response variable, as well as the effects of interactions between factors on the response variable [30], in this study experiments are conducted on 4 factors each in 3 levels, factors such as glucose concentration, microwave power, cholesterol%, surfactant% (Spam, Tween). Based on the

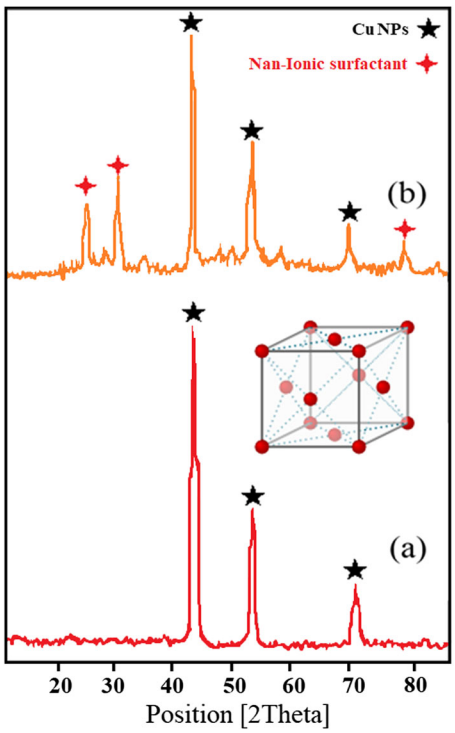

Fig. 2 XRD pattern of of Cu NPs (**a**) and Cu nanospheres embedded in niosomes (**b**)

information obtained from Taguchi method which is shown in Fig. 1, the statistical results show that size of the products is directly related to glucose concentration and microwave power, the percentage of cholesterol and surfactant have little impact on the final product size.

Results and Discussion

In this study Cu nanoparticles were synthesized at different concentrations of glucose, according to below equation (Eq. 1) glucose as a green capping reductant provide electrons to reduce Cu^{2+} ionic to Cu metallic nanoparticles.

$$Cu^{2+} + C_6H_{12}O_6 + H_2O\,Cu + C_6H_{12}O_7 + 2H^+ \quad (1)$$

In this work it was predicted with an increase in the concentration of glucose as a reducing agent, reduction rate will be more, so the number of precipitating metallic clusters increases steeply.

In the recent decades researches have shown that types of vitamins in the herbs have a positive effect on cancer patients [31]. The soy bean plant extracts are popularly recommended for cancer patients [32]. Currently, their rule seems many common herbals such as green tea, grape seed extract, ginger, curcumin and artemisinin have high effect on the treatment of various cancers [33, 34]. Hence by increasing nucleation, the particle size becomes smaller and by increasing the number of particles with a high surface to volume ratio, adhesion occurs. X-ray diffraction (XRD) is one of the most important non-destructive tools to analyze all kinds of matter ranging from fluids to powders and crystals. In order to examine the phase structure and the purity of the products X-ray diffraction at scan range of $10 < 2\theta < 80$ was used, peaks can be perfectly indexed to the face-centered cubic (FCC) crystalline structure Cu NPs and readily indexed as (111), (200), and (220) crystal planes, Fig. 2a, b show XRD patterns of Cu NPs and Cu nanospheres embedded in non-ionic surfactant-based vesicle respectively. XRD pattern obtained from Cu^0 reduced particles from Cu^{2+} shows no other crystalline phases were detected in this pattern.

The crystalline size and diameter (Dc) of Cu NPs nanoparticles can be determined from the diffraction patterns from the full width of the half maximum (FWHM) with the Debay–Scherer equation about 160–180 nm (Eqs. 2–4) [35]:

$$D_{xrd} = 0.9\lambda/\beta\cos\theta \quad (2)$$

where β is the width of the observed diffraction line at its half intensity maximum, K is taken about 0.9, and λ is the wavelength of X-ray source used in XRD. The plot shows in Cu nanospheres embedded in non-ionic surfactant-based vesicle there is the uniformity of the distribution of nanoparticles with the particle size of 120–150 nm that are almost accommodation with SEM and TEM images. All

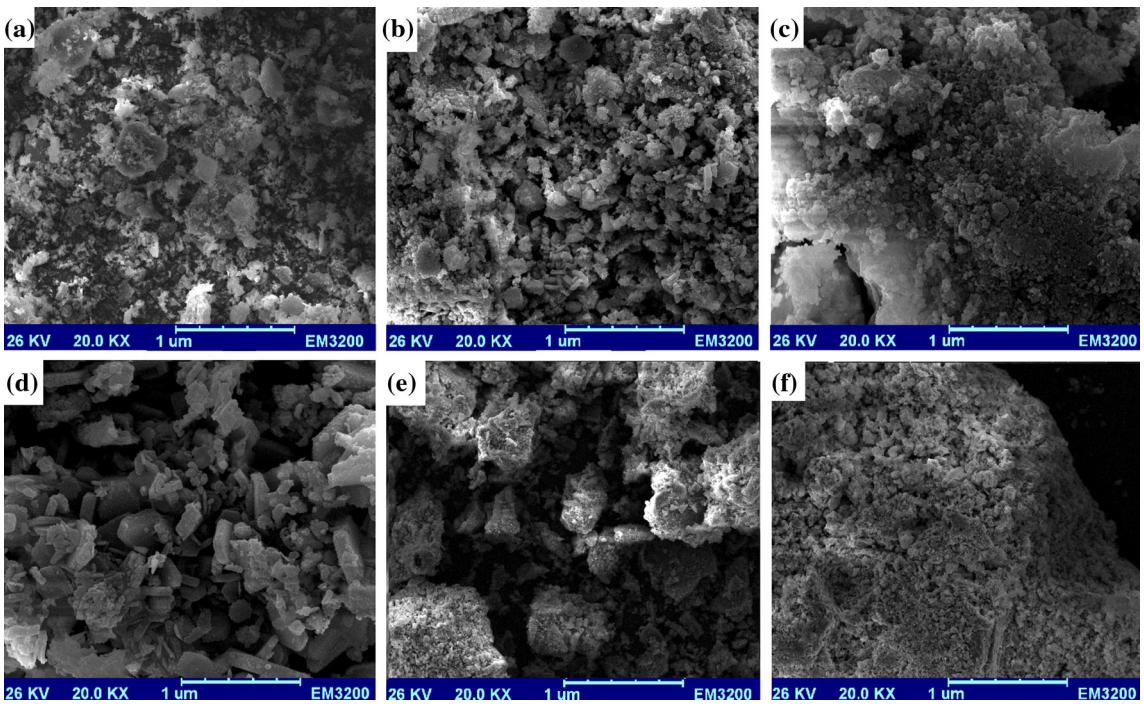

Fig. 3 SEM images of Cu nanospheres embedded in niosomes related to formulations $C_{50}S40_{25}T40_{25}$ (**a**), $C_{50}S60_{25}T60_{25}$ (**b**), $C_{50}S80_{25}T80_{25}$ (**c**), $C_{30}S40_{35}T40_{35}$ (**d**), $C_{30}S60_{35}T60_{35}$ (**e**) and $C_{30}S80_{35}T80_{35}$ (**f**)

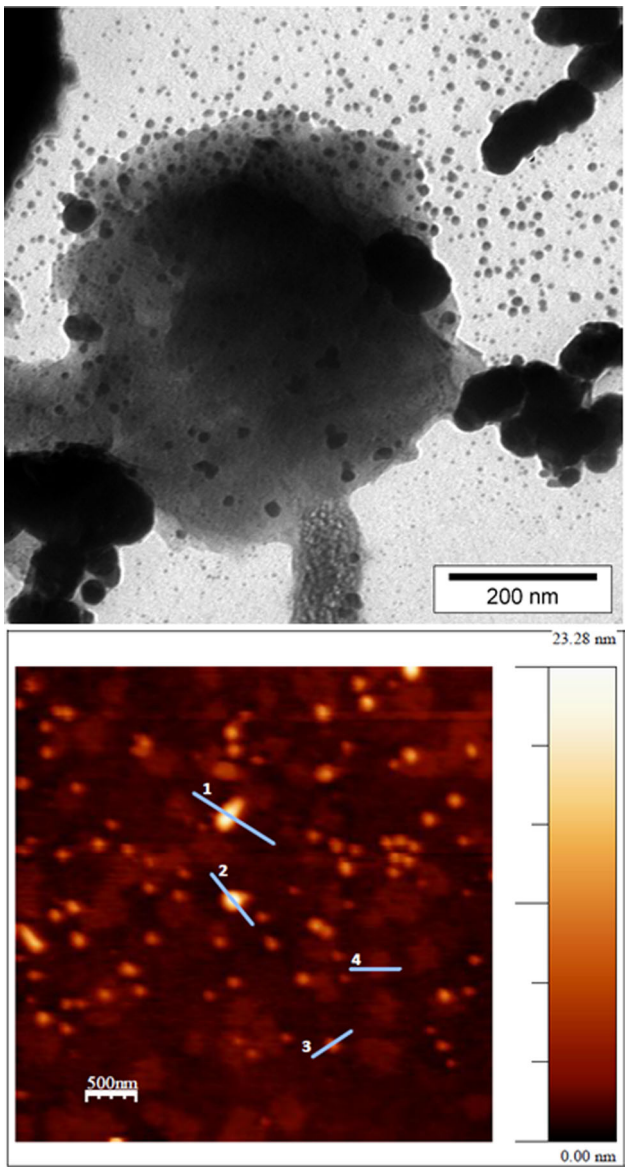

Fig. 4 TEM image of Cu nanoparticles embedded in niosomes related to C30S4035T4035 formula (upper), AFM image sample no. 3 of the synthesized Cu nanoparticles embedded in niosomes (bottom)

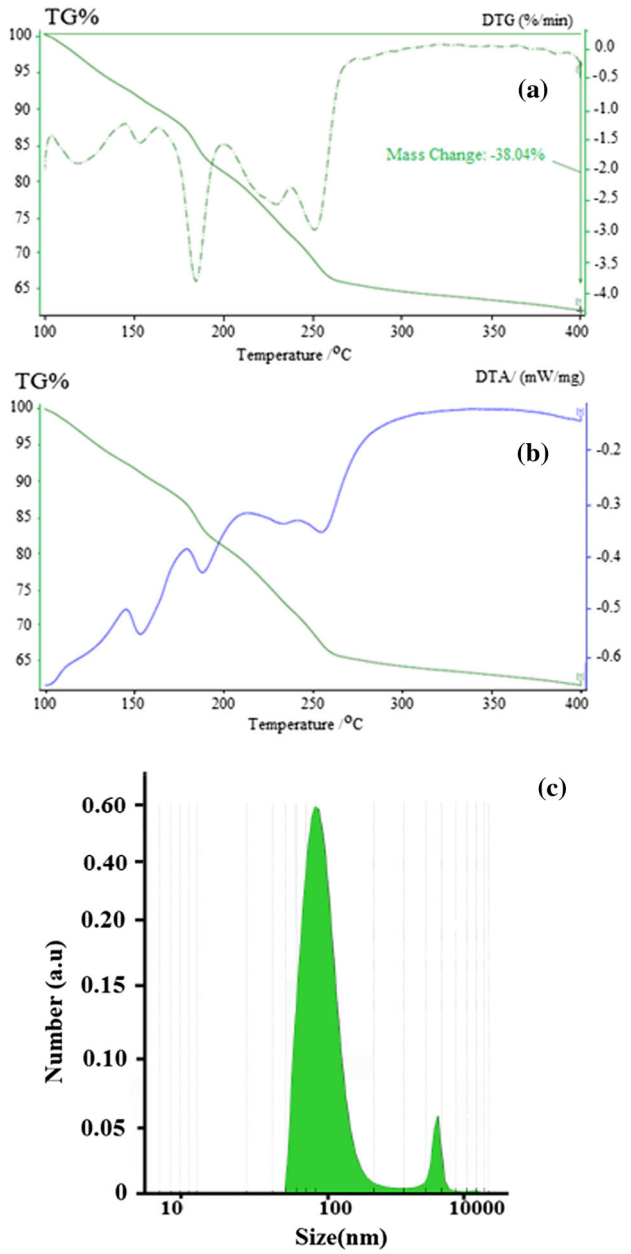

Fig. 5 TG/DTG (**a**), TG/DTA (**b**) and DLS (**c**) analysis of the synthesized Cu nanoparticles embedded in niosomes

measurements were carried out at 25 °C, SEM images of Cu nanospheres embedded in non-ionic surfactant-based vesicle showed in Fig. 3. Scanning electron microscopy and transmission electron microscopy were used to study of morphology and distribution on the structural form of Cu nanoparticles embedded in non-ionic surfactant-based vesicle. SEM images show that new form of nanostructures were particles separately but agglomerated in some areas, this is due to an increase in the surface-to-volume ratio and the activation of the surface of the particles in the bonding of each other. Elemental mapping of Cu nanoparticles embedded in non-ionic surfactant-based vesicle by SEM images is shown in Fig. 3a–f, related to formulations of $C_{50}S40_{25}T40_{25}$, $C_{50}S60_{25}T60_{25}$, $C_{50}S80_{25}T80_{25}$, $C_{30}S40_{35}T40_{35}$, $C_{30}S60_{35}T60_{35}$ and $C_{30}S80_{35}T80_{35}$ respectively. According to SEM images, the particles size and distribution in low irradiation and low concentration of glucose are agglomerate, when irradiation time and concentration increased form of nanostructures were particles separately.

TEM image of Cu nanoparticles embedded in non-ionic surfactant-based vesicle related to $C_{30}S40_{35}T40_{35}$ formula is shown in Fig. 4(upper). TEM image has a good agreement with the size of the nanostructures obtained from the Scherer equation and the scanning electron microscope

images. Atomic force microscopy (AFM) is a microscopic technique imaging of surface area topography and serves as a complementary analysis to determine the size of the particle size. The AFM image of Cu nanospheres embedded in non-ionic surfactant-based vesicle shown in Fig. 4(bottom).

The results confirm that the distribution of nanoparticles with the particle size of 80–110 nm. Figure 5a, b show the TG/DTG and TG/DTA analysis of the synthesized Cu nanoparticles embedded in non-ionic surfactant-based vesicle respectively. DTG describes the decomposition of the constituents of organic matter at specific temperature, whereas, in DTA, the material under study and an inert reference are made to undergo identical thermal cycles, while recording any temperature difference between sample and reference, It can be seen that there are three weight-loss events the first weight-loss is placed in a temperature range of ∼ 50 to 200 °C and is related to water evaporation, weight-loss between temperatures of ∼ 200 and 260 °C assigned to the degradation of Cu nanoparticles, the final stage of weight-loss of structures is after 260 °C assigned to the degradation of nanoparticles embedded in non-ionic surfactant-based vesicle. Dynamic Light Scattering (DLS) as a physical and non-destructive method used to determine the distribution sizes of metallic nanoparticles or quantum dots particles in solutions and suspensions. The velocity of the motion of particles is related to their size (the Stokes–Einstein equation), so that the browning of larger particles is more relaxed than the browning of smaller particles. Dynamic light scattering diagram of Cu nanospheres is shown in Fig. 5c. The particle size of the nanostructures is in the range of 80–120, which is in agreement with the SEM and XRD data. Glucose as a green capping agent in addition to the prevents agglomeration can form various chemical bonds with metal components, thus enhancing the stability of the NPsUV/Vis spectroscopy is essentially used in analytical chemistry and biological macromolecules for the quantitative determination of reflecting variation of % absorbance, such as transition metal ions, highly conjugated organic compounds.

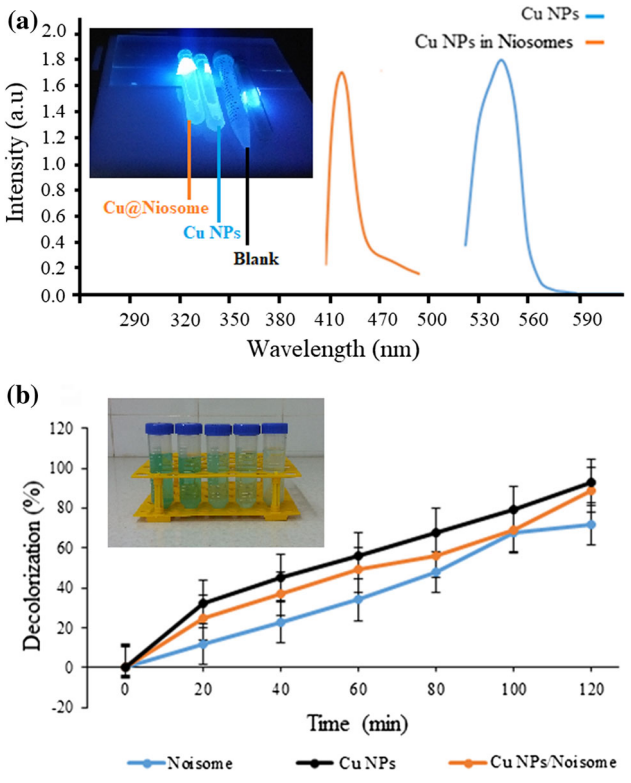

Fig. 6 The UV–Vis spectrum of Cu NPs (blue line) and Cu nanospheres embedded in niosomes (orange line) respectively (**a**) and photodegradation of methylene blue (MB) under UV illumination blank (CuNPs), orange (CuNPs@noisome) and blue (noisome) at 30 min, 60 min, 90 min (**b**) (Color figure online)

The fundamental absorption edge in most nanocomposites and compounds follows the exponential law, through the absorption data the band gap value can be estimated by Tauc's relationship, according to below equation (Eq. 3) [36]. The calculated amount for band gap were 2.2 eV and 2.7 eV for Cu NPs and Cu nanospheres embedded in non-ionic surfactant-based vesicle respectively.

$$\alpha = \alpha(h\nu - Eg)n/h\nu \tag{3}$$

where α is absorption coefficient, hν is the photon energy, α and h are the constants, E_g is the optical band gap of the material, and n depends on the type of electronic transition and can be any value between 1/2 and 3 [37]. Figure 6a shows the UV–Vis spectrum of Cu NPs and Cu nanospheres embedded in niosomes respectively. The absorption edge at 542 nm is related to copper nanoparticles, a broadband around 447 nm is related to Cu nanospheres embedded in non-ionic surfactant-based vesicle. We have also detected the fluorescence emission of the Cu nanoparticles and Cu nanospheres embedded in non-ionic surfactant-based vesicle by a UV-lamp with λ_{ex} = 366 nm light. The blueshift observed in UV–Vis spectrum could be due to Cu nanospheres embedded in non-ionic surfactant-based vesicle are smaller than copper nanoparticles alone, because smaller nanostructures have more the blueshift. The photodegradation of MB rate on the surface of Cu nanospheres embedded in non-ionic surfactant-based vesicle as photocatalytic nanocomposites was calculated by the following equation (Eq. 4):

$$\text{Degradation rate}\ (\%) = \frac{A0 - A}{A0} \times 100 \tag{4}$$

where A_0 and A are initial concentration and changed absorbencies of dye after ultraviolet irradiation, respectively. Degradation diagrams of methylene blue (MB)

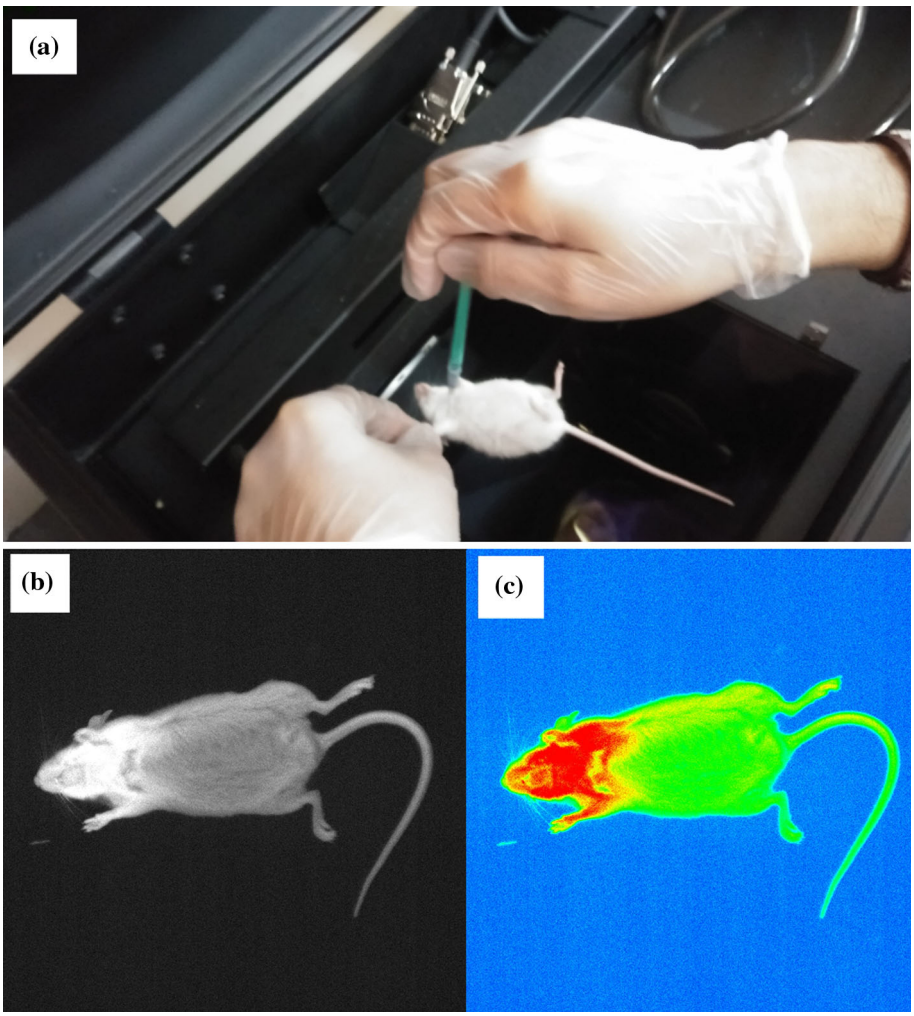

Fig. 7 Injection of 20 µl Cu NPs to neck area mice (**a**) in vivo imaging for Cu nanospheres embedded in niosomes in 1% w/v (**b**, **c**)

under UV illumination for noisome as blank sample, Cu NPs and Cu nanospheres embedded in non-ionic surfactant-based vesicle suspension was displayed at 20 min, 30 min, 40 min, 60 min, 80 min, 100 min, 120 min in Fig. 6b. It can be seen that the presence of Cu nanospheres have major effect on MB decolorization. After 120 min the photocatalytic decolorization MB for noisome as blank sample, Cu NPs and Cu nanospheres embedded in non-ionic surfactant was 72%, 93% and 88%. Cu nanospheres embedded in non-ionic surfactant-based vesicle suspension due to suitable distribution particles have high efficiency for the decolorization MB. Formation of various metal–oxygen bonds such as Cu–O promotes photocatalytic activity of MB. mechanism of the catalytic photocatalytic decolorization of the methylene blue summarized in equation (Eqs. 5–7)

$$e^- + O_2 \rightarrow O_2^{\circ -} \tag{5}$$

$$h^+ + H_2O \rightarrow H^+ + OH^{\circ} \tag{6}$$

$$\text{Methylene blue} + OH^{\circ} \text{ or } O_2^- \rightarrow \text{Degradation products} \tag{7}$$

In this study we have successfully explored a novel theranostic platform based on Cu nanospheres embedded in non-ionic surfactant for investigation of in vivo imaging effects of Cu nanospheres embedded in non-ionic surfactant in the mice (Balb/c male Inbred rats purchased from Animal care center aged between 8 and 6 weeks) were feeded and raised according to the Institutional Animal Care and Use Committee (IACUC) protocol. After anesthetizing the mouse with 5 cc 1:2 ketamine/xylazine we injected 20 µl Cu nanospheres embedded in non-ionic surfactant to neck area mice since the light emitted after the passage of the internal organs the body, as well as the visible tissue of the body, is valuable in the study of biological species. The resulting image shows that nanoparticles have good spatial properties in light emission from the neck tissue. In vivo imaging for Cu nanospheres embedded in niosomes in 1% w/v indicated in Fig. 7 this nano sampler will be a convenient and applicable

replacement for chemotherapy-based therapies. On the other hand, this nanoparticle can be used in the biomedical and pharmaceutical industry for diagnostic and imaging purposes simultaneously with targeted therapy. We propose the use of Cu nanostructures which synthesized with green chemistry in the photocatalytic activity of MB and also imaging of the living organism study as a new way to eliminate toxic and carcinogenic compounds such as ethidium bromide in vivo imaging. Magnetic resonance imaging is a promising noninvasive imaging approach for preoperative staging of breast cancer and monitoring tumor response to therapy.

About the mechanism, clinical studies our results suggest that cancer cells can be detected by conjugated Cu nanospheres embedded in non-ionic surfactant-based vesicle to glucose structures and tracking these structures in the body. The metal nanoparticles have high potential as molecularly targeted, dual modality imaging agents for in vivo imaging of cancer treatment. The Cu nanospheres with photocatalytic activity trough photodynamic therapy (PDT) act as an emerging, non-invasive therapeutic strategy that involves photosensitizer (PS) drugs and external light for the treatment of cancer.

Conclusion

In this study for the first time, Cu nanospheres embedded in non-ionic surfactant-based vesicle were synthesized by coprecipitation assisted microwave method, we used glucose as a green capping to reduce Cu^{2+} ionic to Cu metallic nanoparticles, products were characterized by X-ray, SEM, TEM, DLS, TGA and UV–Vis spectrum. Non-ionic surfactant-based vesicle as carriers for drug delivery can be embedded Cu nanoparticles to create antibacterial, targeted trace and optical properties. Approximate size of nanostructures was estimated 80–110 nm with Debay–Scherer equation that confirmed by SEM and TEM images. This new nanostructure which suspended in vesicles can be used in many applications in the field of drug delivery, biomedical imaging, cancer therapy, and chemical sensing.

Acknowledgements Authors are grateful to council of Pharmaceutics Research Center, Institute of Neuropharmacology, Kerman University of Medical Sciences, Kerman, Iran.

Funding This work was supported by the Pharmaceutics Research Center, Institute of Neuropharmacology, Kerman University of Medical Sciences, Kerman, Iran.

Compliance with Ethical Standards

Conflict of interest All authors declare that they have no conflict of interests.

Human and Animal Rights This article does not contain any studies with human participants performed by any of the authors. Animals purchased from Animal care center were feeded and raised according to the Institutional Animal Care and Use Committee (IACUC) protocol.

References

1. D. Ag Seleci, M. Seleci, J.-G. Walter, F. Stahl, and T. Scheper (2016). Niosomes as nanoparticular drug carriers: fundamentals and recent applications. *J. Nanomater.* **43**, 243–256.
2. D. Akhilesh, K. Bini, and J. Kamath (2012). Review on span-60 based non-ionic surfactant vesicles (niosomes) as novel drug delivery. *Int. J. Res. Pharm. Biomed. Sci.* **3**, 6–12.
3. Z. S. Bayindir and N. Yuksel (2010). Characterization of niosomes prepared with various nonionic surfactants for paclitaxel oral delivery. *J. Pharm. Sci.* **99**, 2049–2060.
4. H. Ai, S. A. Jones, and Y. M. Lvov (2003). Biomedical applications of electrostatic layer-by-layer nano-assembly of polymers, enzymes, and nanoparticles. *Cell Biochem. Biophys.* **39**, 23–35.
5. R. Esfand and D. A. Tomalia (2001). Poly (amidoamine)(PAMAM) dendrimers: from biomimicry to drug delivery and biomedical applications. *Drug Discov. Today* **6**, 427–436.
6. K. Grage, A. C. Jahns, N. Parlane, R. Palanisamy, I. A. Rasiah, J. A. Atwood, and B. H. Rehm (2009). Bacterial polyhydroxyalkanoate granules: biogenesis, structure, and potential use as nano-/micro-beads in biotechnological and biomedical applications. *Biomacromolecules* **10**, 660–669.
7. V. P. Torchilin (2007). Micellar nanocarriers: pharmaceutical perspectives. *Pharm. Res.* **24**, 1–13.
8. S. Honary and F. Zahir (2013). Effect of zeta potential on the properties of nano-drug delivery systems-a review (Part 2). *Trop. J. Pharm. Res.* **12**, 265–273.
9. N. S. Thakur, G. Patel, V. Kushwah, S. Jain, and U. C. Banerjee (2018). Self assembled gold nanoparticle-lipid nanocomposites for on-demand delivery, tumor accumulation, and combined photothermal-photodynamic therapy. *ACS Appl. Bio Mater.* **23**, 678–789.
10. S. E. Skrabalak, J. Chen, L. Au, X. Lu, X. Li, and Y. Xia (2007). Gold nanocages for biomedical applications. *Adv. Mater.* **19**, 3177–3184.
11. J. Zeng, X. Xu, X. Chen, Q. Liang, X. Bian, L. Yang, and X. Jing (2003). Biodegradable electrospun fibers for drug delivery. *J. Control. Release* **92**, 227–231.
12. X. Michalet, F. Pinaud, L. Bentolila, J. Tsay, S. Doose, J. Li, G. Sundaresan, A. Wu, S. Gambhir, and S. Weiss (2005). Quantum dots for live cells, in vivo imaging, and diagnostics. *Science* **307**, 538–544.
13. M. Ahmed and A. Ghanem (2014). Chiral β-cyclodextrin functionalized polymer monolith for the direct enantioselective reversed phase nano liquid chromatographic separation of racemic pharmaceuticals. *J. Chromatogr. A* **1345**, 115–127.
14. M. Ahmed, M. M. A. Yajadda, Z. J. Han, D. Su, G. Wang, K. K. Ostrikov, and A. Ghanem (2014). Single-walled carbon nanotube-based polymer monoliths for the enantioselective nano-liquid chromatographic separation of racemic pharmaceuticals. *J. Chromatogr. A* **1360**, 100–109.
15. Y. Zhu, S. Murali, M. D. Stoller, A. Velamakanni, R. D. Piner, and R. S. Ruoff (2010). Microwave assisted exfoliation and reduction of graphite oxide for ultracapacitors. *Carbon* **48**, 2118–2122.

16. L. Lv, X. Bian, J. Zhou, G. Zhu, P. Liu, X. Chen, and Q. Liu (2010). Synthesis of $NiFe_2O_4$ nanocrystalline with various size by hydrothermal method. *J. Synth. Cryst.* **4**, 31–48.
17. A. R. Karimi, Z. Alimohammadi, J. Azizian, A. A. Mohammadi, and M. J. Mohammadizadeh (2006). Solvent-free synthesis of tetrasubstituted imidazoles on silica gel/NaHSO4 support. *Catal. Commun.* **7**, 728–732.
18. P. R. Arya, P. Jha, and A. K. Ganguli (2003). Synthesis, characterization and dielectric properties of nanometer-sized barium strontium titanates prepared by the polymeric citrate precursor method. *J. Mater. Chem.* **13**, 415–423.
19. D. Macwan, P. N. Dave, and S. Chaturvedi (2011). A review on nano-TiO_2 sol–gel type syntheses and its applications. *J. Mater. Sci.* **46**, 3669–3686.
20. P. V. Kumar, S. Pammi, P. Kollu, K. Satyanarayana, and U. Shameem (2014). Green synthesis and characterization of silver nanoparticles using *Boerhaavia diffusa* plant extract and their anti bacterial activity. *Ind. Crops Prod.* **52**, 562–566.
21. R. Riahi-Madvaar, M. A. Taher, and H. Fazelirad (2017). Green and microwave synthesis of $SrAl_2O_4$ nanoparticles by application of pomegranate juice: study and characterization. *Appl. Nanosci.* **7**, 913–917.
22. M. N. Nadagouda, T. F. Speth, and R. S. Varma (2011). Microwave-assisted green synthesis of silver nanostructures. *Acc. Chem. Res.* **44**, 469–478.
23. H. Ammar, M. Haider, M. Ibrahim, and N. El Hoffy (2017). In vitro and in vivo investigation for optimization of niosomal ability for sustainment and bioavailability enhancement of diltiazem after nasal administration. *Drug Deliv.* **24**, 414–421.
24. A. Hussain, A. Samad, S. Singh, M. Ahsan, M. Haque, A. Faruk, and F. Ahmed (2016). Nanoemulsion gel-based topical delivery of an antifungal drug: in vitro activity and in vivo evaluation. *Drug Deliv.* **23**, 642–657.
25. J. Somagoni, C. H. Boakye, C. Godugu, A. R. Patel, H. A. M. Faria, V. Zucolotto, and M. Singh (2014). Nanomiemgel-A novel drug delivery system for topical application-in vitro and in vivo evaluation. *PLoS ONE* **9**, 115–122.
26. M. Jin, G. He, H. Zhang, J. Zeng, Z. Xie, and Y. Xia (2011). Shape-controlled synthesis of copper nanocrystals in an aqueous solution with glucose as a reducing agent and hexadecylamine as a capping agent. *Angew. Chem. Int. Ed.* **50**, 10560–10564.
27. C. Dufes, F. Gaillard, I. F. Uchegbu, A. G. Schätzlein, J.-C. Olivier, and J.-M. Muller (2004). Glucose-targeted niosomes deliver vasoactive intestinal peptide (VIP) to the brain. *Int. J. Pharm.* **285**, 77–85.
28. S. Moghassemi and A. Hadjizadeh (2014). Nano-niosomes as nanoscale drug delivery systems: an illustrated review. *J. Control. Release* **185**, 22–36.
29. Y. A. Youssef, Y. Beauchamp, and M. Thomas (1994). Comparison of a full factorial experiment to fractional and Taguchi designs in a lathe dry turning operation. *Comput. Ind. Eng.* **27**, 59–62.
30. K. E. Taylor, R. J. Stouffer, and G. A. Meehl (2012). An overview of CMIP5 and the experiment design. *Bull. Am. Meteor. Soc.* **93**, 485–498.
31. S.-Y. Yin, W.-C. Wei, F.-Y. Jian, and N.-S. Yang (2013). Medicine A: therapeutic applications of herbal medicines for cancer patients. *Evid. Based Complement. Altern. Med.* **13**, 56–68.
32. C. Amaral, M. R. T. Toloi, L. D. Vasconcelos, M. J. V. Fonseca, G. Correia-da-Silva, and N. J. Teixeira (2017). The role of soybean extracts and isoflavones in hormone-dependent breast cancer: aromatase activity and biological effects. *Food Funct.* **8**, 3064–3074.
33. B. Gerber, C. Scholz, T. Reimer, V. Briese, and W. J. Janni (2006). Complementary and alternative therapeutic approaches in patients with early breast cancer: a systematic review. *Breast Cancer Res. Treat.* **95**, 199–209.
34. J. Tavakoli, S. Miar, M. M. Zadehzare, and H. J. Akbari (2012). Evaluation of effectiveness of herbal medication in cancer care: a review study. *Iran. J. Cancer Prev.* **5**, 144–156.
35. M. Salavati-Niasari and F. Davar (2009). Synthesis of copper and copper (I) oxide nanoparticles by thermal decomposition of a new precursor. *Mater. Lett.* **63**, 441–443.
36. H. Zhang, Z. Ji, T. Xia, H. Meng, C. Low-Kam, R. Liu, S. Pokhrel, S. Lin, X. Wang, and Y.-P. Liao (2012). Use of metal oxide nanoparticle band gap to develop a predictive paradigm for oxidative stress and acute pulmonary inflammation. *ACS Nano* **6**, 4349–4368.
37. G. Ren, D. Hu, E. W. Cheng, M. A. Vargas-Reus, P. Reip, and R. P. Allaker (2009). Characterisation of copper oxide nanoparticles for antimicrobial applications. *Int. J. Antimicrob. Agents* **33**, 587–590.